Neutron diffraction bulk texture study with impact properties correlation of electron beam welded dissimilar Fe-7%Al alloy to steel joints

Soumitra Kumar Dinda[1*], Winfried Kockelmann[2], Gour Gopal Roy[3], Prakash Srirangam[4]

[1]Materials Science and Engineering, University of Toronto, Canada

[2]Rutherford Appleton Laboratory, ISIS Facility, United Kingdom

[3]Metallurgical and Materials Engineering, Indian Institute of Technology Kharagpur, India

[4]Warwick Manufacturing Group, University of Warwick, United Kingdom

*Corresponding author: soumitra.dinda@utoronto.ca, 184 College Street, Toronto, Ontario, Canada, M5S3E4, T: +1 647-656-8248

Abstract

Present work focused on the crystallographic bulk texture study of dissimilar Fe-7percentage Al alloy to mild steel joints by electron beam welding using Time-of-flight neutron diffraction technique. Textural properties directly correlated with V-notch Charpy impact study. Different processing conditions like the use of beam oscillation and by changing welding speed on texture change and its impact on the performance of the joint was evaluated. Neutron diffraction was performed using general materials diffractometer beamline at ISIS neutron radiation source. Texture analysis and their variation obtained in terms of pole-figures, inverse pole figures and orientation distribution functions (ODFs). Beam oscillation shows a uniform and ordered textured grains in both fusion zone (FZ) and heat-affected zone (HAZ) due to more heat mixing that reduced unidirectional solidification gradient. ODFs study reveals more gamma fibre components in both FZ and HAZ compared to its non-oscillating counterparts and higher welding speed joints, which predominantly shows more Goss, rotated Goss and cube/ alpha fibre components. Charpy impact-strength shows approximately 60 % improvement in value for the joints, which was prepared by using beam oscillation whereas 20 % reduction for higher welding speed condition. Also, X-ray tomography study of Charpy broke sample showed very lesser and shallow cracks

and in smaller volume percentage of 0.45 compared with joints produced by the non-oscillating beam showing maximum value of 2.99 %.

Keywords: Electron beam welding, Beam Oscillation, Neutron diffraction, Bulk texture, Charpy impact test, X-ray computed tomography,

1. Introduction

Neutron diffraction is well established for spatially resolved measurements of the bulk texture of materials due to deep penetration approximately 1 cm^3 which provides a unique possibility to examine bulk properties and coarse-grained structures [1]. Neutron diffraction widely used for most of the engineering materials. Here at constant scattering angle, the polychromatic beam used to have a lot of detectors attached with it. Time of flight (TOF) neutron diffraction unique advantages for texture study because here both orientation space and reciprocal lattice act simultaneously in a single scanning [2]. Textural study of weld products is most important to understand and to optimize welding parameters for getting the best quality products in terms of performance of the joints. Dissimilar metals combination like Fe-7% Al alloy to mild steel is gaining importance in different sectors especially in aerospace and automotive sectors because of light-weighting as it decreases fuel consumption and to reduce green-house CO_2 emissions [3]. Aluminium addition to steel, effectively reduces its density like here only 7–8% aluminium to steel reduces approximately 17% its density [4]. Electron beam welding (EBW) is a special type of fusion state joining process which justified by low heat input, higher power density, high penetration and high depth to width ratio and fewer defects in the joints [5, 6]. During the welding process, metal undergoes through the complex thermal cycle and plastic flow which affects mechanical properties within fusion and HAZ regions that could be affected by grains orientation and texture from its original base metals which were typical rolling textures [8, 9]. Some researchers worked on the same topic not precisely related to EB-welding of Fe 7% Al alloy to steel joints but worked on textural analysis

by electron diffraction and neutron diffraction with mechanical properties correlation, and it's discussed below.

Eghlimi *et al.*, (2015) worked on the textural analysis of gas tungsten arc welded duplex stainless steel (SS) to austenitic SS by electron backscatter diffraction (EBSD) study. They did observe texture and base metal grain boundary distribution to its change in HAZ regions because of the formation of annealing twins and γ & β-FCC fibres components in SS HAZ through recrystallization process. Brokmeier *et al.,* (2007) worked on laser welded dissimilar 5083 Al alloy to 6013 Al alloy joints to characterize the crystallographic texture by electron backscatter diffraction (EBSD), hard X-ray and neutron diffraction techniques. They observed finer grains of 5083 Al-alloys, which produced weak deformation texture. They also found the welding process produced cube texture components with minor <100> fibre texture in welding direction. Kar *et al.*, (2016) worked on EB-welded Cu-stainless steel dissimilar joints and concluded that beam oscillation is an effective method to increase joint strength significantly. Lindau *et al.*, (2011) worked on EB-welded ferritic-martensitic steel and performed mechanical properties characterization like tensile, Charpy impact at both before and after weld heat treatment. They justified the changes in the mechanical properties and also correlated with that of change with micro and nanostructure. Rao *et al.*, (2008) did multi-pass bead-over-bead EB-welded joints like two and three passes of Ti-6Al-4V alloys to modify fracture toughness and Charpy impact strengths. They observed in the reduction of toughness value of conventional stringer bead welded products rather than from its base metal properties. Lan *et al.*, (2012) analyzed martensite-austenite (M-A) constitute and its effect on toughness value of low C-bainitic steel welded by submerged arc welding. Initiation energy of HAZ cracks significantly decreased due to the presence of M-A constituent, which mainly helps to form cleavage cracks. But, in HAZ, the presence of prior austenitic grains significantly reduced that propagation energy. *Shin et al.,* (2015) worked on shielded metal arc (SMA) and flux cored arc welded (FCAW) structural steel joints for Charpy impact and hardness study with microstructural

observations. Authors found SMA-welded joints HAZ had much higher low-temperature impact toughness rather than FCAW joints. *Hamid et al.*, (2018) studied on post weld heat-treatment (PWHT) on the physical properties and mechanical performance of S275J2 SMA-welded C-steel joints and concluded that PWHT decreased hardness value. Microstructural observation shows that the increase in grain size of the fusion region increases Charpy impact strength.

It is evident from the literature study and research review articles, bulk texture at individual locations of the joints like both HAZ and fusion zone with mechanical properties correlation like Charpy impact strength of the dissimilar Fe-7 percentage Al alloy to mild steel welding especially by electron beam welding process does not any researchers examined until now. Also welding parameters like oscillating beam and by varying scanning speed and its effect on textural properties no one did.

2. Experimental observations

2.1. Materials and Electron beam welding

Fe-Al alloy (C = 0.0044 %, Al = 6.94 %, Mn = 0.20%, Fe= rest) and mild steel (C= 0.3 %, Al= 0.08 %, Mn = 0.92 %, Si = 0.23%, Fe = rest) plates chosen for material combinations and nominal chemical composition were performed by X-ray spectroscopy (XPS) analysis.

Table 1*:* EB-welding processing parameters used in present study.

Joint No	Applied voltage (kV)	Operating current (mA)	Scanning speed (mm/min)	Oscillation details	
				Diameter	Frequency
Joint 1	70	110	1000	-	-
Joint 2	70	120	1000	1.0 mm	600 Hz
Joint 3	70	130	1500	-	-

Both materials having a dimension of 100 mm × 50 mm with 5 mm thickness were cut from full provided materials and make ready by series of polishing with an acetone cleaning. For butt-welding of dissimilar

combination Fe7%Al alloy to mild steel, 60 kV - 12 kW EBW machine had used with a set of processing condition from the previous experience and with by trail and run process for getting full penetration by changing beam current in minor level and welding parameters chosen here listed in *Table 1*.

2.2. Neutron diffraction

Neutron diffraction experiment was performed using the general materials diffractometer (GEM) at ISIS neutron source, Rutherford Appleton Laboratory (RAL), UK. GEM is mainly a diffractometer acts at high count rate to observed structures for both crystalline and glassy materials [18]. Five analysis points were selected on every joint, which included both base materials, both side HAZ and fusion region as represented in *Fig. 1(a).*

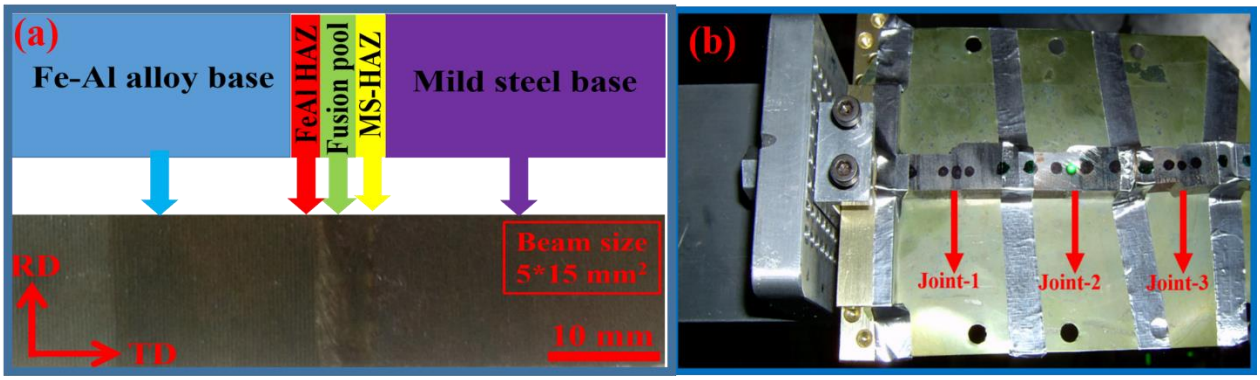

Fig. 1. (a) Scan point noted different sections. ***(b)*** Welds fixing of all joints, beam direction was parallel to the normal, perpendicular to rolling & transverse direction.

For the data collection, weld materials were mounted on a translation stage in the GEM vacuum chamber. The neutron wavelength range during the measurements was maintained 0.2 to 3.5 Å. Neutron beam size set to 5x15 mm^2 with the orientation of the beam used it for all the cases. All materials set up within the system quite tough, and here it shows in *Fig. 1(b)* where a total of three samples were fixed in a straight-line form as mentioned in that figure. Data sets were collected for one sample orientation, with the incident beam (normal to the sample plate) transmitting the 5 mm thick material. Each data set was collected for about 47 minutes for each analysis point. The diffraction data were analysed by the

material analysis using diffraction (MAUD) software tool [19], which is capable of analyzing texture data of multi-detector neutron diffractometer. With MAUD, list of parameters can determine such that phase fractions, lattice parameters and ODFs etc. Raw data were collected and normalized according to the incident neutron flux distribution, and it corrected for detector efficiencies. For each analysis point, normalized data converted into 164 d-spacing patterns. Each of these 164 patterns corresponds to a detector group that covers an angular range of about 10^0 x 10^0. All 164 spacing was then Rietveld fitted in MAUD, with ODF cells defined and refined by the Extended WIMV (E-WIMV) algorithm. E-WIMV can handle perfectly incomplete and highly irregular pole figure coverages [19]. For the perfect instrument resolution, we selected 10^o for the ODF cell size. Due to joints absorption anisotropy and to minimize the sample displacement effects on the structure and texture parameters, list of parameters were refined here [18], i.e. both material displacement parameters, one TOF absorption coefficient, monitor counts, which were associated scale factor for individual detector groups, and background parameters. As for the phase and structure parameters, the following refinement strategy was followed. Phase fractions were refined where more than one phase was observed. Cell parameters were refined for major phases where significant Bragg peak was observed above background. Lattice parameters were kept fixed for minor phases, for example for the Fe-Al phase (2.8899 Å) in the mild steel HAZ and steel (2.8665 Å) in the Fe-Al HAZ. Both phases having BCC crystal structure having same space group (Im-3m). An empirical value of 0.8 $Å^2$ was used for the Debye-Waller parameter for the steel and Fe-Al alloy phases. MTEX [20] in Matlab was used to obtain final PFs, IPFs and ODFs of the different regions of the joints for better comparison and representation.

2.3. V-notch Charpy impact study

Charpy impact test, popularly known as Charpy V-notch test, which is characterized by standardized high strain-rate, determine the total energy amount absorbed by a standard material due to impact fracture. This experiment provides both quantitative and qualitative information of the materials. The

quantitative result from this experiment is the energy required to be a fracture of a material, which is the fundamental way to measure the toughness value of any materials. Regarding qualitative results from this study, the ductility of the material can be inferred from the fracture surface of the material. [21]. Here Charpy impact testing was performed by using 400J maximum capacity impact testing Instron® machine. ASTM-23 standard sub-size specimen were prepared keeping the interface region at middle position [22]. Since fusion zones narrow in nature, notches were carefully made such that the entire notch line lies within the fusion zone area. Three tests were carried out for each weld-conditioned joint and take the average energy value to minimize the errors. As the thickness of the samples were sub-standard, impact energy first normalized according to ASTM standard and then impact energy strength calculated by the following reaction.

$$I = \left(\frac{P}{A}\right) \ldots\ldots\ldots\ldots\ldots\ldots\ldots\ldots\ldots\ldots \text{Eq. } 1$$

Where, I = Impact strength in J/cm^2.

P = Absorbed energy by any material during the experiment in Joules.

A = Cross-section area below the intentionally made notch before experiment in cm^2.

2.3.1. X-ray computed tomography (XCT) fracture surface study

XCT was carried out for Charpy fracture cracks comparison among all three joints using the Zeiss Versa 520 system. XCT is the 3D non-destructive qualitative and quantitative observation method to identify any defects that arises during the fracture test. Al-alloy side broken side taken for test and it placed a table between the X-ray source and detector. As the table is rotating, during X-ray switch it on, X-ray will either pass or attenuate by the material. This will give result to form a grey-scale radiograph on the detector screen behind. Scan resolution calculated by the object magnification factor that results to form the relative position of the detector geometry. Sets of such radiography projections were taken

throughout the full 360^0 rotations and then reconstructed the 3D volume by back projection. Scanning parameter is chosen here listed in *Table 2* below.

Table 2: Parameters used for XCT scanning for cracks study.

Parameters	Values for cracks study
Voltage (kV)	110
Current (µA)	140
Exposure (ms)	1000
Number of projections	1800
Optical magnification	20X
Voxel size (µm)	29.95

3. Results and discussion

3.1. TOF bulk texture analysis

The textures in terms of PFs, IPFs & ODFs were determined by the E-WIMV method in MAUD. We consider three non-collinear planes (111), (200) and (220) or its parallel planes.

3.1.1. Both base metals

The texture from both base metals used for welding shows typical recrystallized rolling texture. *Fig. 2* shows the characteristics of the parent materials and by virtue, BCC in nature. In terms of comparison of both materials crystal orientation, it is evident that in case of Fe-Al alloy, stronger pole density is observed along 210, 311, 110 II ND and very less along 111 II ND which gives less deformation during any thermo-mechanical treatment [23]. Whereas in case of mild steel, maximum grains are oriented 111, 110 II ND and less in 001 II ND that helps easy dislocations movement because of more closed pack slips systems. Higher the pole density higher the probability of finding planes II ND.

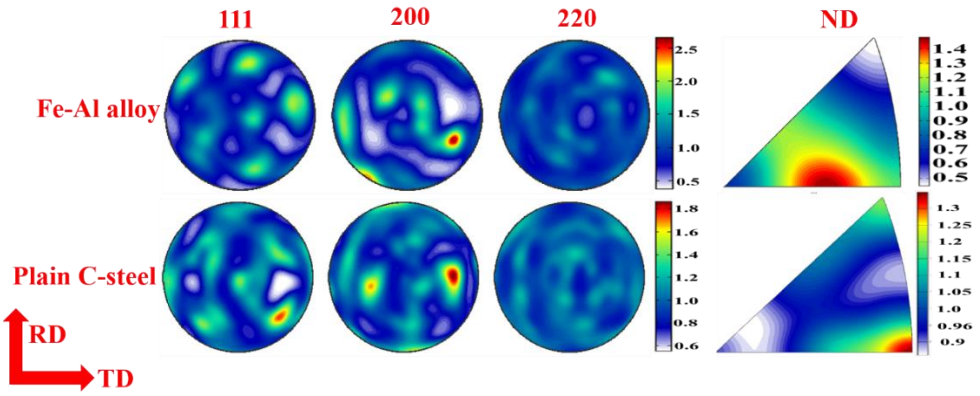

Fig. 2. PFs & IPFs of both base metal FeAl alloy (top) and mild steel (bottom).

3.1.2. Fe-Al BCC phase in Fe-Al HAZ & steel BCC phase in mild steel HAZ regions

Fig. 3(a) shows the variation of PFs and IPFs of FeAl BCC phase in FeAl alloy HAZ side and *Fig. 3(b)* represents for steel BCC phase in mild steel HAZ side for all three joints respectively. In contrast with *Fig. 2*, the PFs & IPFs in both HAZ shows significantly different texture.

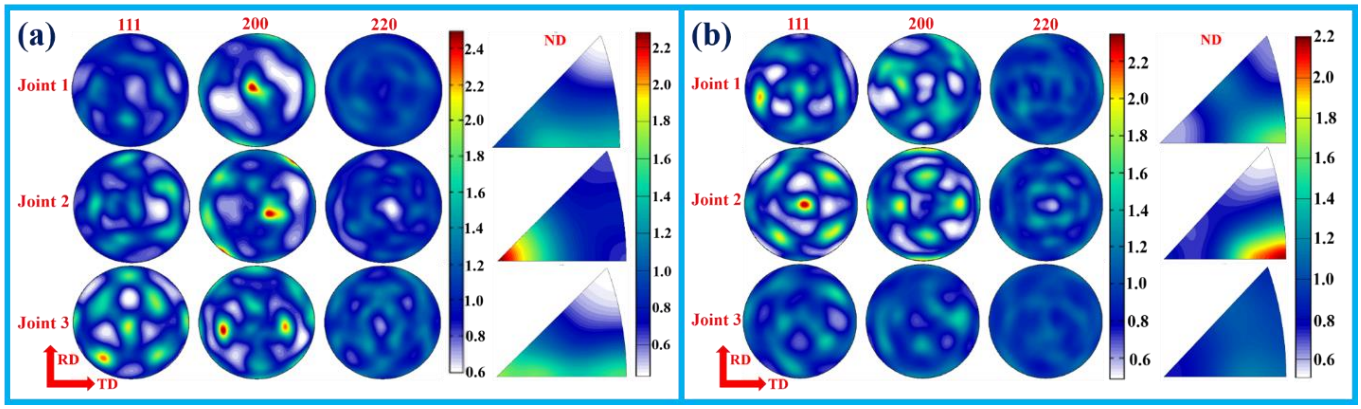

Fig. 3. PFs & IPFs of ***(a)*** Fe-Al BCC phase of Fe-Al side HAZ, ***(b)*** steel BCC phase of mild steel side HAZ. N.B. all are scaled for the same m.r.d.

For Fe-Al BCC phase in Fe-Al HAZ regions of the joints (Fig. 3 (a)), Joint 2 showing more stronger pole densities along 010 & 110 II ND where average along 111 II ND but other two joints (Joint 1 & Joint 3) very fewer grains are oriented along 111 II ND tends to zero whereas found some grains are oriented along 101, 210 001 II ND direction. Stronger m.r.d. values along 111 compared to 200 & 220 means more elongation before going to fracture during any thermo-mechanical treatment. From *Fig. 3*

(b), for Joint 3, no stronger pole densities are observed in comparison with other the two Joints. For Joint 1, maximum is oriented along 010, 211 II ND whereas in case of Joint 2 maximum is oriented along 010, 211 II ND. Cell parameters, phase weight % and maximum multiples of a random distribution (m.r.d.) are listed in *Table 3.* For the Fe-Al HAZ, the steel phase fraction is very small, and therefore the unit cell parameter was kept fixed (2.8665 Å), i.e. not refined during the analysis.

Table 3: PFs comparison for both FeAl-HAZ and mild steel HAZ of all three joints.

Regions		Fe-Al HAZ regions			Mild steel HAZ regions		
Joint No	Type	Phase %	Max. m.r.d.	Cell parameters (error)	Phase	Max. m.r.d.	Cell parameter (error)
Joint 1	FeAl-BCC	99.999	2.65	2.8859 (1)	6.99	-	2.8899 (fixed)
	Steel-BCC	0.0001		2.8665 (fixed)	92.01	2.19	2.8784 (1)
Joint 2	FeAl-BCC	99.999	1.52	2.8964 (1)	13.62	-	2.8899 (fixed)
	Steel-BCC	0.0001		2.8665 (fixed)	86.37	2.46	2.8786 (1)
Joint 3	FeAl-BCC	96.60	3.78	2.8907 (1)	0.001	-	2.8899 (fixed)
	Steel-BCC	3.40		2.8665 (fixed)	99.999	1.61	2.8760 (1)

Quantitative comparison for Fe-Al HAZ, limiting diffusion of steel phase took place due to the difference in materials properties and diffusion of aluminium in steel. We note that every case steel phase fraction tends to negligible. We assume that the mild steel-HAZ includes small regions of the FeAl-BCC phase that have a small number of FeAl-BCC crystallites. Hence Bragg reflections for FeAl-BCC were present at a few angles but not present in all diffraction detectors, which was why the Rietveld fit returned a zero-phase fraction overall. *Table 4* also shows quantitative information of mild steel HAZ regions of the joints and found that tiny amount of FeAl BCC phases are present as similar to Fe-Al HAZ side but variation noticeable. Majority of FeAl BCC phases found for Joint 2 (13 %), and it is very less approximately zero in case of Joint 3.

3.1.3. Fusion regions

Fig. 4(a) shows PFs and IPFs comparison of FeAl BCC phase & (b) steel BCC phase in fusion regions for all three joint systems. For Joint 2 in FeAl HAZ region, pole densities are higher along in 111, 010, 320 II ND where average along 001, 211, 210, 111 II ND and very less along 331, 010 II ND whereas in case of Joint 1, maximum pole densities are in 210, 010, 211, 311 II ND and very less along 001, 111 II ND. For Joint 3 systems, the more mixed type texture we found. Maximum pole densities are in 010, 210, 211 II ND and a less along 001, 331,111 II ND. Similarly, in mild steel HAZ region, Joint 2 having more grains along 111, 320 II ND, few along 001, 211 II ND and very less along 331, 221 II ND but in case of Joints which shows more along 010 II ND and very less along 111, 331 II ND.

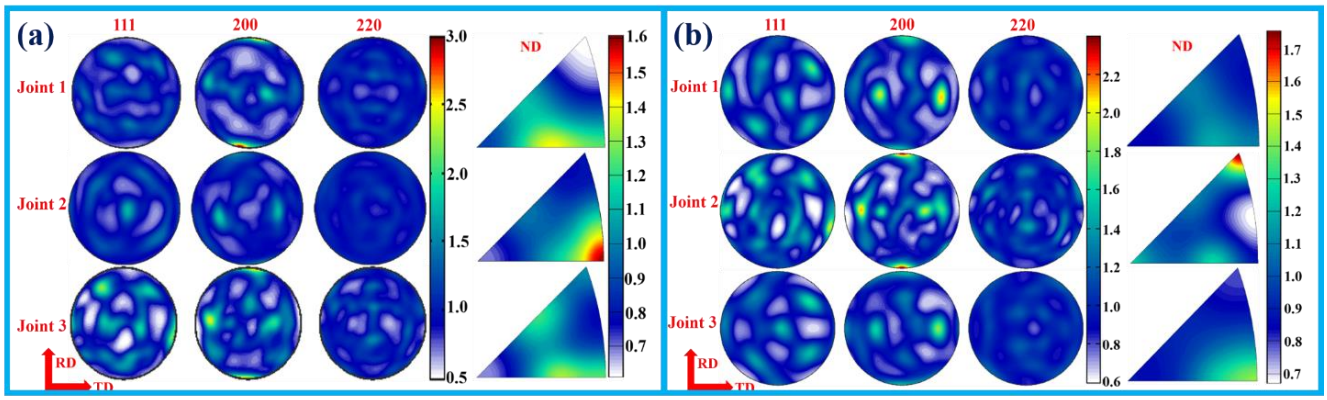

Fig. 4. (a) PFs & IPFs of Fe-Al BCC phase ***(b)*** steel BCC phase of fusion regions of the joints. N.B. all are scaled for the same m.r.d.

Quantified comparison of phases present at fusion regions at different weld processing conditions shown in *Table 4.* There seems to be more steel in fusion regions for Joint 2 (58 %) compared to Joint 1 (38 %) and it lowest for Joint 3 (30%), however, this could be due to beam oscillation phenomena promotes better mixing of alloying elements n fusion regions of the joints. In the FZ, all cell parameters are refined due to the significant amount of all phases present.

***Table 4*:** PFs comparison for fusion regions among all three joints.

Joint No	Type	Phase	Max. m.r.d.	Cell parameter (error)
Joint 1	FeAl-BCC	61.93	2.27	2.8891 (1)
	Steel-BCC	38.07	2.81	2.8774 (1)
Joint 2	FeAl-BCC	41.47	1.82	2.8842 (1)
	Steel-FCC	58.53	1.78	2.8756 (1)
Joint 3	FeAl-BCC	69.78	2.64	2.8869 (1)
	Steel-BCC	30.22	2.44	2.8757 (1)

3.1.4. ODFs variation among all three joints

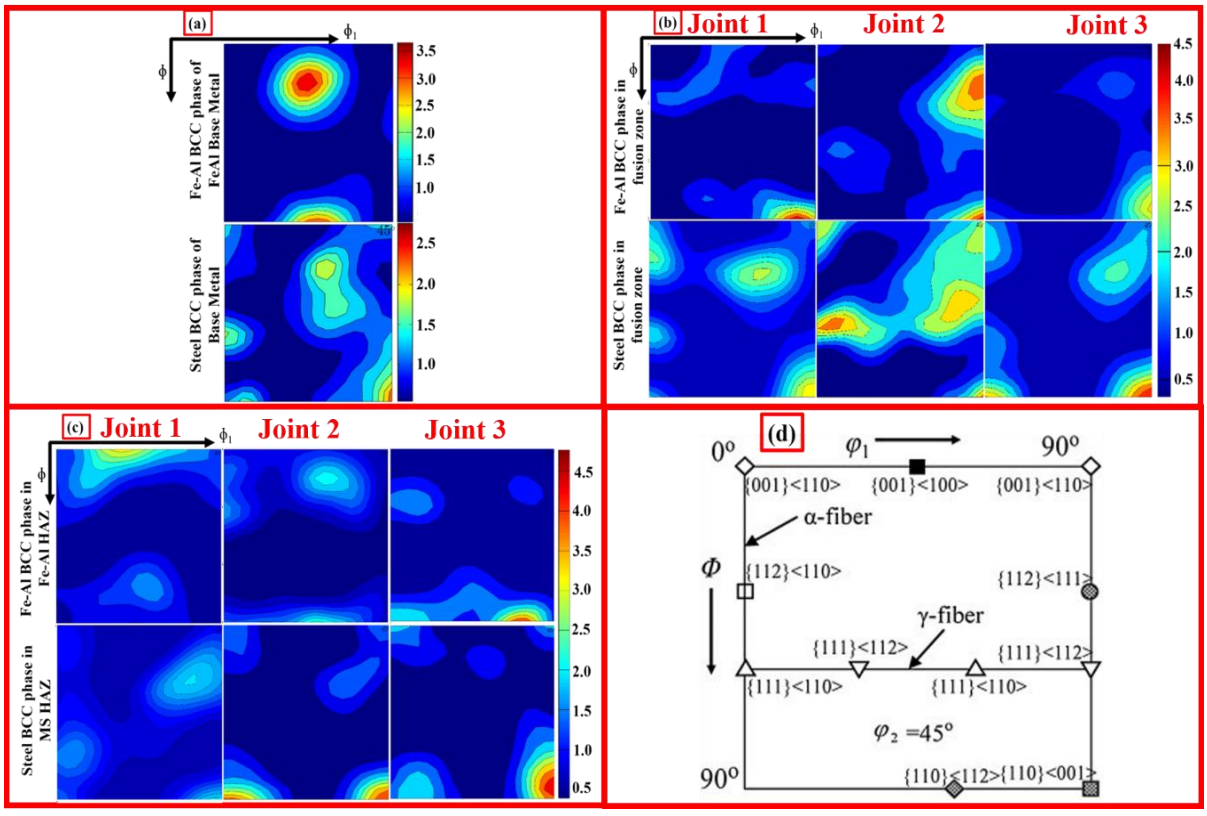

Fig. 5. ODFs represented here (i.e. Φ, Φ_1 = 0°–90° & $\Phi_2 = 45^0$ sections of the Euler space) (a) both base, (b) both HAZs and (c) fusion regions; (d) $\Phi_2 = 45^o$ of Euler space orientation in ferritic steel.

Orientation distribution function (ODF) study of all three regions, i.e. both base metals, both HAZ, fusion zone represented here of all the joints in the form of $\varphi_2 = 45^0$ in Euler space in *Fig 5*. In fusion region, Joint 2 showed strong gamma-fiber texture (<111> // ND) compared to Joint 1 and Joint 3 which showed Goss ({011} <001>), rotated Goss and cube ({001} <110>) fiber texture of both BCC phase (Fe-Al BBC & steel BCC). In both HAZ, no noticeable texture variation among all three joints was observed only small Goss components observed for Joint 2 and Joint 3. Apart from microstructure, grain orientation and their distribution at the HAZs and FZ of the joints significantly influence the properties of joints like elastic moduli, impact strength, percentage elongation, fatigue and fracture toughness. Both base metals having BCC rolling texture, commonly described in terms of two fibres components, i.e. α and γ fibres. The α fibre has <110> II to RD and includes {110} <011>, {112} <011> and {111} <110> while γ fibre is partial fibre component with {111} parallel to ND includes {111} <112> and {111} <110>. Fusion area exhibits solidification texture, commonly described in terms of <001> parallel to ND. During solidification, grain prefers to grow with <001> since heat flow is easier along that direction in cubic lattice. Texture orientation changes due to directional and non-directional solidification phenomena happened at mainly fusion region of the joints during the solidification process. The intense stirring produced by an oscillating beam with churning effect decreased unidirectional solidification resulting from forming more randomized texture and with more γ and α fibre component compared to joint made without oscillation. The γ fibre components are the most deformable fibre component, which promotes to help easy dislocations movement due to having more closed pack slip systems. Increase in welding speed in the absence of beam oscillation, chances to form more columnar grains towards cooling direction lead to form more cube and Goss fibre components intensity.

3.2. V-notch Charpy impact study

3.2.1. Charpy strength of joints

Bar chart comparison of strength shows in *Fig. 6 (a)* among all three joints and both base metals and it's found that impact strength of Joint 2 (133 J/cm^2) shows maximum value, minimum for Joint 3 (66 J/cm^2) and in between for Joint 1 (83 J/cm^2) as shown in *Table 5* in details. It shows approximately 60 % improvement in strength value compared to without oscillating joints. Improper melting due to higher speed and irregular distribution at the fusion region may be attributed to the reduction in fracture strength at higher welding speed joint. For better understanding about the fracture mechanism, scanning electron microscopy fractographs analysis was carried out, and it shows all over the ductile mode of fracture everywhere having deep and small dimple cleavage shown in *Fig. 6 (b)*. Only for Joint 3 it shows some quasi-cleavage type fractures (yellow circle). Dimple size also calculated taking at least 800-900 dimple in account form several images of all three test samples at same magnification level and found that maximum for Joint 2 (3726.6 nm) compared to Joint 1 (3167.9 nm) and lowest for Joint 3 (3167.9 nm).

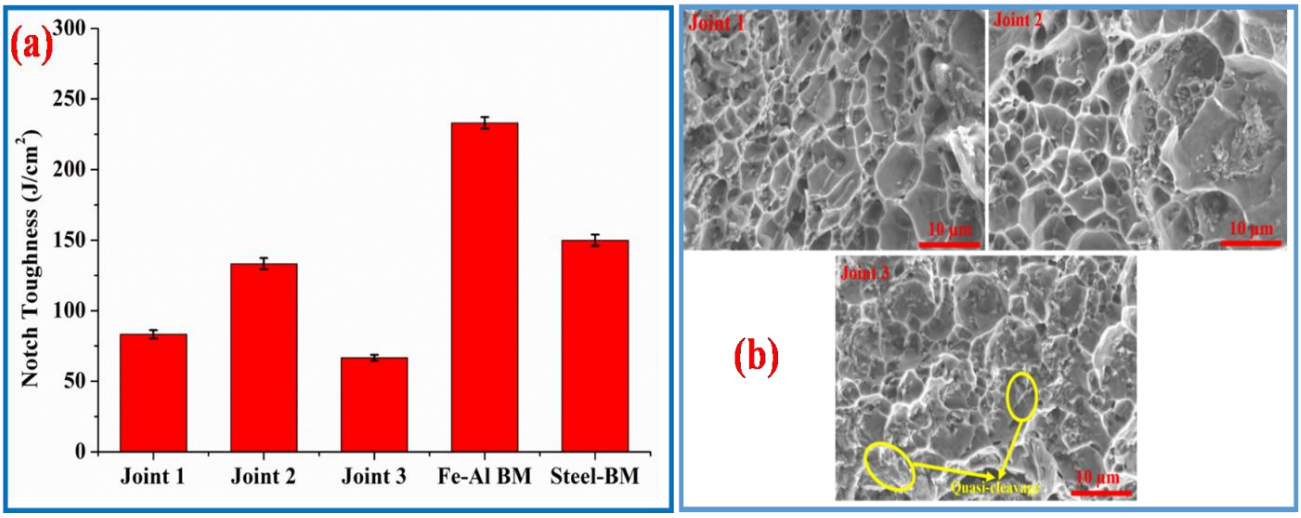

Fig. 6 (a). Charpy impact strength bar chart, ***(b)*** fractography comparisons.

Table 5: Charpy impact results for all joints and base metals conducted at room temperature.

Joints No	Energy absorbed (J)	Energy Normalized to standard (J)	C/S area at notch (cm^2)	Impact strength (J/cm^2)	% improvement in impact strength
Joint 1	5 ± 1.5	16.65 ± 1.5	0.20	83.25 ± 3	Reference
Joint 2	8 ± 2	26.67 ± 2	0.20	133.35 ± 4	60 %
Joint 3	4 ± 1	13.33 ± 1	0.20	66.65 ± 2	-20%
FeAl BM	14 ± 2	46.62 ± 2	0.20	233.1 ± 4	-
MS BM	9 ± 2	30 ± 2	0.20	150 ± 4	-

3.2.2. XCT Crack phenomena study of Charpy broke specimens

Fig. 7 (a) represents the X-ray tomography image study of Charpy broken samples of one side of the materials (Fe-Al alloy side) showing the presence of cracks and its orientation throughout the materials. For clear visualization, only cracks are also represented without material matrix shown in *Fig. 7 (b)*.

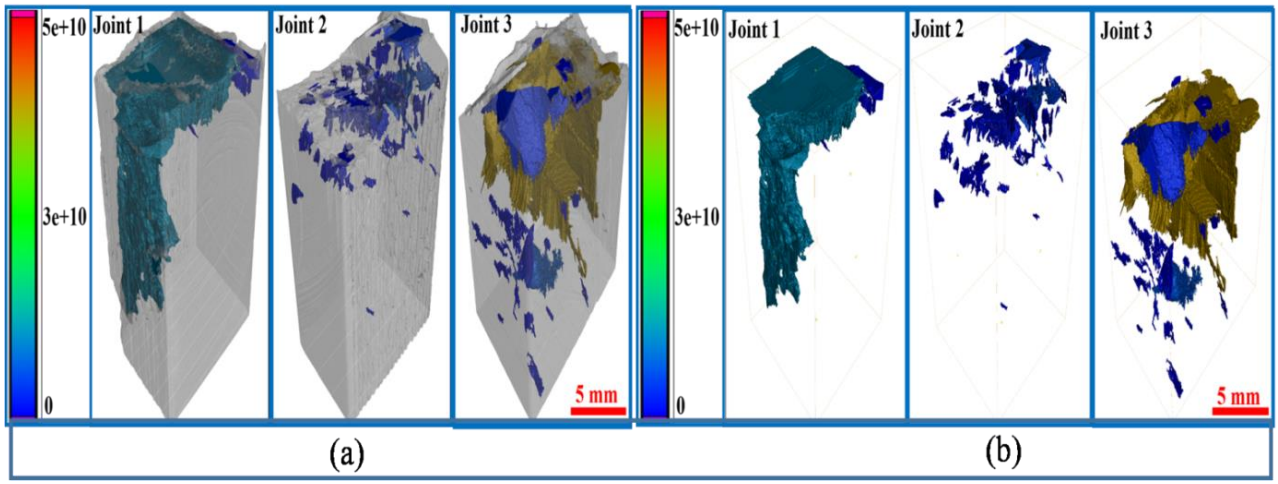

Fig. 7 (a). Reconstructed 3D transparent fracture cracks with matrix, ***(b)*** only cracks without matrx for all joints.

By different colour coding concerning crack size easily differentiate different size and shaped cracks with the materials. Joint 2 (with oscillation case) show small size cracks compared to Joint 1 (without

oscillation) by blue colour coding. By increasing welding speed (Joint 3), it seems to increase the crack length progressively. For proper cracks information, quantitative results also tabulated in *Table 6.*

Table 6: Shows tabulated cracks quantification information of all three joints.

Joint No	Average surface area (mm^2)	Average volume (mm^3)	Number of cracks	% volume formed
Joint 1	62.162	1.602	7	2.99
Joint 2	2.139	0.033	53	0.45
Joint 3	9.138	0.146	35	1.36

The result shows the average surface area, average volume, crack number and more importantly % crack volume of the total scan area. Joint 2, which was prepared at with oscillation condition, provides very less average surface area and volume compared to the other two joints. Beam oscillation effectively reduces the chance to form more significant size cracks in the materials. Volume % cracks within of the total scan area were also lowest for Joint 2 (0.45 %) and found maximum value for Joint 3 (1.36 %), which was prepared at higher welding speed condition. The number of cracks for Joint 2 shows the highest value but very small in average size, which justified by the smallest volume % of the total scan area.

4. Conclusions

Dissimilar combination of Fe-7percentage Al alloy to mild steel joints by electron beam welding process successfully carried out at different welding conditions and characterized by neutron diffraction bulk texture study with impact properties correlation. Major summaries from the above studies pointed out here below.

- Beam oscillation creates more textured grains in the weld seam due to better heat mixing, thus reduced unidirectional temperature/thermal gradients. In addition, churning action provides a more homogenized

mixing of alloying elements. ODFs study shows more gamma fibre components for oscillation beam in fusion zone whereas, in both HAZ regions, Goss fibre components lead to giving deformable properties.

- Increasing welding speed produced more directional texture due to higher cooling rate, and fibre components found major cube and alpha, which are not suitable fiber components for the mechanical performance of the joints.
- Texture results directly correlated with notched Charpy impact properties of the joints and found that maximum impact strength at oscillation condition with the largest dimple size fracture and lowest for higher welding speed condition joints.
- XCT results for fracture crack shows 3D visualization and quantification of small and shallow cracks mainly formed for Joint 2, whereas the other two joints show large and deeper cracks within the materials itself. Average surface area, average volume and % volume formation least for oscillation joints which also strengthen our observations.

Acknowledgements

Authors gratefully acknowledge UKERI (UK-India collaborative project) (Grant no. EP/1002456/1) for the financial help to carry out research work in RAL, UK.

5. References

1. Han W, Ukai S, Wan F, Sato Y, Leng B, Numata H, Oono N, Hayashi S, Tang Q, Sugino Y (2012) Hardness and Micro-Texture in Friction Stir Welds of a Nanostructured Oxide Dispersion Strengthened Ferritic Steel. Materials Transactions 53:390–394. https://doi.org/10.2320/matertrans.M2011226
2. Wenk H-R (2002) Texture and Anisotropy. Reviews in Mineralogy and Geochemistry 51:291–329. https://doi.org/10.2138/gsrmg.51.1.291
3. Dinda SK, Srirangam P, Roy GG (2019) Effects of beam oscillation on porosity & intermetallic compounds formation of electron beam welded DP600 steel to Al-5754 alloy joints. Materials,

Metals & Materials Society 239-249. https://doi.org/10.1007/978-3-030-05861-6_21.

4. Dinda SK,, Sk Md. B, Roy GG, Srirangam P (2016) Microstructure and mechanical properties of electron beam welded dissimilar steel to Fe – Al alloy joints. Materials Science & Engineering A 677:182–192. https://doi.org/10.1016/j.msea.2016.09.050
5. Bandi B, Dinda SK, Kar J, Roy GG, Srirangam P (2018) Effect of weld parameters on porosity formation in electron beam welded Zircaloy-4 joints: X-ray tomography study. Vacuum 158:172–179. https://doi.org/10.1016/j.vacuum.2018.09.060
6. Dinda SK, Kar J, Jana S, Roy GG, Srirangam P (2019) Effect of beam oscillation on porosity and intermetallics of electron beam welded DP600-steel to Al 5754-alloy. Journal of Materials Processing Technology 265:191–200. https://doi.org/10.1016/j.jmatprotec.2018.10.026
7. Kar J, Roy SK, Roy GG (2018) Influence of beam oscillation in electron beam welding of Ti-6AL-4V. International Journal of Advanced Manufacturing Technology 94:4531–4541. https://doi.org/10.1007/s00170-017-1169-1
8. Gangil N, Maheshwari S, Siddiquee AN, Abidi MH, El-Meligy MA, Mohammed JA (2019) Investigation on friction stir welding of hybrid composites fabricated on Al-Zn-Mg-Cu alloy through friction stir processing. Journal of Materials Research and Technology 8:3733–3740. https://doi.org/10.1016/j.jmrt.2019.06.033
9. Dong J, Zhang D, Luo X, Zhang W, Zhang W, Qiu C (2020) EBSD study of underwater friction stir welded AA7003-T4 and AA6060-T4 dissimilar joint. Journal of Materials Research and Technology. https://doi.org/10.1016/j.jmrt.2020.02.056
10. Eghlimi A, Shamanian M, Eskandarian M, Zabolian A, Szpunar JA (2015) Characterization of microstructure and texture across dissimilar super duplex/austenitic stainless steel weldment joint by austenitic filler metal. Materials Characterization 106:208–217. https://doi.org/10.1016/j.matchar.2015.05.036

11. Brokmeier H-G, Lenser S, Schwarzer R, Ventzke V, Riekehr S, Kocak M, Homeyer J (2007) Crystallographic texture of dissimilar laser welded Al5083-Al6013 sheets. THERMEC 2006, Pts 1-5 539–543:3894–3899. https://doi.org/10.4028/www.scientific.net/MSF.539-543.3894
12. Kar J, Roy SK, Roy GG (2016) Effect of beam oscillation on electron beam welding of copper with AISI-304 stainless steel. Journal of Materials Processing Technology 233:174–185. https://doi.org/10.1016/j.jmatprotec.2016.03.001
13. Lindau R, Klimenkov M, Jäntsch U, Moslang A, Commin L (2011) Mechanical and microstructural characterization of electron beam welded reduced activation oxide dispersion strengthened - Eurofer steel. Journal of Nuclear Materials 416:22–29. https://doi.org/10.1016/j.jnucmat.2011.01.025
14. Rao KP, Angamuthu K, Srinivasan PB (2008) Fracture toughness of electron beam welded Ti6Al4V. Journal of Materials Processing Technology 199:185–192. https://doi.org/10.1016/j.jmatprotec.2007.08.001
15. Lan L, Qiu C, Zhao D, Gao X, Du L (2012) Analysis of martensite-austenite constituent and its effect on toughness in submerged arc welded joint of low carbon bainitic steel. Journal of Materials Science 47:4732–4742. https://doi.org/10.1007/s10853-012-6346-x
16. Shin HS, Park KT, Lee CH, Chang KH, Do VNV (2015) Low temperature impact toughness of structural steel welds with different welding processes. KSCE Journal of Civil Engineering 19:1431–1437. https://doi.org/10.1007/s12205-015-0042-8
17. Hamid A, Nurhasan N, Darmawan AS, Fitri M, Rahmat B (2018) Mechanical and physical properties improvement of S275J2 welded carbon steel. AIP Conference Proceedings 1977:. https://doi.org/10.1063/1.5042938
18. Kockelmann W, Chapon LC, Radaelli PG (2006) Neutron texture analysis on GEM at ISIS. Physica B: Condensed Matter 385-386 I:639–643. https://doi.org/10.1016/j.physb.2006.06.091

19. Wenk H-R, Lutterotti L, Vogel SC (2010) Rietveld texture analysis from TOF neutron diffraction data. Powder Diffraction 25:283–296. https://doi.org/10.1154/1.3479004
20. List M, Guide U, Overview F (2018) MTEX Toolbox (/)
21. Mathur KK, Needleman A, Tvergaard V (1994) 3D analysis of failure modes in the Charpy impact test. Modelling and Simulation in Materials Science and Engineering 2:617–635. https://doi.org/10.1088/0965-0393/2/3A/014
22. ASTM (2007) Norma E23-07a - Standard Test Methods for Notched Bar Impact Testing of Metallic Materials. American Society for Testing and Materials Handbook 14:28. https://doi.org/10.1520/E0023-07AE01.2
23. Wang C (2014) Dislocations and strengthening mechanisms. Materials Engineering 174–206